Numerical Simulation of Slope and Mountain Flows

RICHARD T. MCNIDER

K. E. Johnson Environmental and Energy Center, The University of Alabama in Huntsville, Huntsville, AL 35899

ROGER A. PIELKE

Department of Atmospheric Sciences, Colorado State University, Fort Collins, CO 80523

(Manuscript received 30 November 1983, in final form 23 June 1984)

ABSTRACT

Early descriptive models of mountain–valley circulations indicated that the mountain flow (i.e., the along-valley axis component out of the valley) is a true three-dimensional phenomenon. According to these descriptions, at night shallow-down slope flows on the valley sidewalls directly driven by temperature deficits near the surface produce a pooling of cool air in the valley. This deep pool of cool air in the valley compared with a much shallower surface inversion over the plains (to which the valley opens) produces a secondary flow (the mountain flow) out of the valley driven by a deep hydrostatic pressure gradient. It is this deep secondary flow which is most important to pollutant transport in deep valleys and which has not been previously investigated in a numerical model.

It is the purpose of this investigation to numerically simulate the above-mentioned secondary circulation using a three-dimensional numerical model. The Colorado State University Hydrostatic Mesoscale Model—a hydrostatic, primitive equation model, forced by a surface energy budget—was utilized for the simulations. Both idealized topography and an actual Colorado valley were used in the investigation to emulate the classic mountain–plain configuration discussed above. Special attention was given to the development of the sidewall slope flows which produce the pooling of air in the valley. Results of the simulations indicated shallow slope flows less than 100 m deep started almost immediately after cooling began and reached their maximum velocity after approximately one hour and then slowly decreased through the night. A high level of turbulence was noted near the top of the slope flows. The turbulence was not only due to shear in the slope flow, but to destabilization of the temperature profile because of thermal advection. Definite pooling of cool air occurred in the valley with cooling occurring at all heights to near ridge tops. The secondary flow out of the valley lagged the development of the slope flows by approximately one hour, but was very deep, filling the whole valley to near ridge height.

1. Introduction

Thermally induced up- and down-valley flows are a common occurrence in well-defined valleys. In the 1930–60 period considerable interest (at least as evidenced in the literature) was directed toward the observation and description of these mountain–valley circulations. Recent air pollution concerns have revised interest in mountain–valley circulations, but in the intervening years comparatively little theoretical or observational work was undertaken. The primary reason for this lull in activity is the fact that the descriptive studies of the early period (Defant, 1951) indicated that the secondary flows along the valley axis flows[1] were a nonlinear, three-dimensional phenomenon dependent upon the three-dimensionality of the valley and intimately related to the sidewall slope flows and radiative and turbulent exchange processes. Such complexity effectively precluded the application of the analytic mathematical tools available at the time. Only in recent years have computer capacity and numerical modeling techniques progressed to the point where full three-dimensional treatment of the problem is possible.

It is the purpose of this investigation to utilize a hydrostatic, primitive equation model to examine specifically the development of the secondary along-valley axis flow in well-defined valleys. Successful modeling of these flows could be a direct assistance in air pollution modeling since it is this secondary flow which is most important to pollutant transport and valley ventilation. Before beginning discussion of the modeled circulations, it is appropriate to provide a historical perspective on the description and theories of mountain–valley circulations.

a. Descriptive models

Much of the early ideas and conceptual models of topographic circulations was rooted in observations

[1] In this investigation, following Defant, *mountain* wind will refer to the along-valley axis component flowing out of the valley and *valley* wind refers to flow up the valley.

taken in European valleys. Defant (1951) provides an excellent description of this work, including the characteristics of slope and mountain–valley flows and the importance of the slope flow in driving the mountain–valley circulations. Defant attributed the slope flow, as one might expect, to the difference in temperature over the inclined slopes and the air at the same altitude over the center of the valley. This produces upslope flow during the day and downslope flow at night. These slope flows are relatively shallow, especially the nocturnal downslope flow, and because they are limited to the valley walls would probably not be a conspicuous feature. However, the mountain–valley flow is much deeper, extending from the valley floor to near the ridge crests of the valley walls. The physical mechanism producing the valley flow, put forward by Defant, is the establishment of a pressure gradient between the valley and the plains outside the valley. The pressure gradient is introduced by the slope winds which gradually fill the valley with cooler (or warmer) air through a greater depth than on the plains. Thus, a deeper flow in the valley is established for which physical generation is less direct than the slope flows. Figure 1 provides a schematic of Defant's descriptive model. Observations in some of the larger European valleys and more recently the work of Whiteman and McKee (1977), show both shallow slope flows and deeper flows along the axis of the valley.

A major consequence of this theory is that the slope of the valley floor is of little consequence to the direction of the along-valley component. The most important features determining the direction of the mountain-valley flow are the direction of the valley opening onto a plain, the slopes of the ridge-tops, and the direction of the widening or narrowing of the valley. The influence of these features on mountain–valley winds are explored in a lively audience discussion contained in a paper by Davidson and Rao (1963).

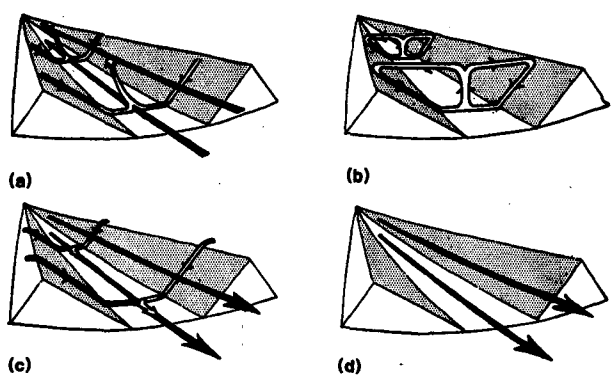

FIG. 1. A schematic of the development of an along-valley mountain wind after Defant (1951). (a) The initial convergence of the slope flows is in the center of the valley superimposed on the remaining afternoon up-valley flow. (b) Gradually the interior of the valley is cooled throughout its depth by the slope flows. (c) This deep pool of cool air compared to a much shallower inversion over the plains outside the valley produces a deep flow toward the valley mouth. (d) The down-valley flow or mountain wind becomes the dominant wind component.

b. Numerical models

Perhaps the most courageous attempt at numerical simulation of these circulations was that of N. H. Thyer in his dissertation in 1962 and also reported later (Thyer, 1966). Thyer, attempting to model particularly steep-walled valleys, encountered innumerable numerical stability problems in several model formulations. He achieved his most success employing a three-dimensional vorticity equation, but, was only able to integrate the model for 120 s of model time. Although his solutions did produce an along-valley axis component, the results would appear questionable given the short time period of the simulation.

More recently, Mahrer and Pielke (1977) simulated large-scale two-dimensional upslope and downslope winds using a different version of the basic hydrostatic, primitive equation model employed in the present investigation. Their study, however, was primarily a simulation study and did not address the details of the slope flows. Yamada (1981) also recently simulated nocturnal drainage flows in a three-dimensional model, but, did not address the along-valley mountain wind. The work of Egger (1981) comes closest to addressing the descriptive ideas of Defant concerning the development of along-valley flow. Egger, using a simpler model and different topography than considered in the present study, did examine flow along the valley axis.

The idealized topography used in the first part of the present study is constructed to examine the essential physics that led early investigators to their descriptive models of mountain–valley flows. For this reason the basic valley configurations have a high height-to-width ratio opening onto a flat plain. It should be emphasized that the purpose of this idealized topography is to compare the numerical model results and the physics producing these results to the physical concepts behind the descriptive models and not to simulate a single set of observations. It is felt that this qualitative compositing of diverse data sets for comparison with the idealized model configuration is useful due to limited data in valleys and the complexity of actual topography.

In the second part of this investigation the model is applied to a deep valley in Colorado where tethersonde data taken by Whiteman (1981) are used to provide more quantitative evaluation of the model.

2. Mesoscale model descriptions

a. Model equations

The basic structure of the mesoscale model used in the present investigation was originally developed

by Pielke (1974) for study of south Florida sea breezes. At the University of Virginia and Colorado State University additional improvements of the model have been made (e.g., Mahrer and Pielke, 1977; McCumber and Pielke, 1981; McNider and Pielke, 1981).

The basic model equations for hydrostatic incompressible flow in terrain following coordinates are given below:

$$\frac{du}{dt} = fv - fV_g - \theta\frac{\partial\tilde{\pi}}{\partial x} + g\frac{z^* - \bar{s}}{\bar{s}}\frac{\partial z}{\partial x}G - g\frac{z^*}{\bar{s}}\frac{\partial s}{\partial x} + \left(\frac{\bar{s}}{s - z_g}\right)^2\frac{\partial}{\partial z^*}\left(K_m\frac{\partial u}{\partial z^*}\right) + \text{Fil}(u), \quad (1)$$

$$\frac{dv}{dt} = -fu + fU_g - \theta\frac{\partial\tilde{\pi}}{\partial y} + g\frac{z^* - \bar{s}}{\bar{s}}\frac{\partial z_G}{\partial y} - g\frac{z^*}{\bar{s}}\frac{\partial s}{\partial x} + \left(\frac{\bar{s}}{s - z_G}\right)^2\frac{\partial}{\partial z^*}\left(K_m\frac{\partial v}{\partial z^*}\right) + \text{Fil}(v), \quad (2)$$

$$\frac{d\tilde{\theta}}{dt} = \left(\frac{\bar{s}}{s - z_G}\right)^2\frac{\partial}{\partial z^*}\left(K_h\frac{\partial\tilde{\theta}}{\partial z^*}\right) + \text{Fil}(\theta) + F_\theta, \quad (3)$$

$$\frac{dq}{dt} = \left(\frac{\bar{s}}{s - z_G}\right)^2\frac{\partial}{\partial z^*}\left(K_h\frac{\partial q}{\partial z^*}\right) + \text{Fil}(q) + F_q, \quad (4)$$

$$\frac{\partial}{\partial t}(s - z_G) + \frac{\partial}{\partial x}u(s - z_G) + \frac{\partial}{\partial y}v(s - z_G) + \frac{\partial}{\partial z^*}w^*(s - z_G) = 0, \quad (5)$$

$$\frac{\partial\tilde{\pi}}{\partial z^*} = -\frac{s - z_G}{\bar{s}}\frac{g}{\tilde{\theta}}, \quad (6)$$

where

$$\tilde{\pi} = c_p\left(\frac{\tilde{P}}{P_{00}}\right)^{R/c_p},$$

$$w^* = \frac{\bar{s}}{s - z_G}w - \frac{z^*}{s - z_G}\left(\frac{\partial s}{\partial t} + u\frac{\partial s}{\partial x} + v\frac{\partial s}{\partial y}\right) + \frac{z^* - s}{s - z_G}\left(u\frac{\partial z_G}{\partial x} + v\frac{\partial z_G}{\partial y}\right),$$

$$\frac{d}{dt} = \frac{\partial}{\partial t} + u\frac{\partial}{\partial x} + v\frac{\partial}{\partial y} + w^*\frac{\partial}{\partial z^*}.$$

TABLE 1. Model parameters and configuration.

Surface roughness	10 cm
Time step	30 s
Latitude	35°N
Horizontal grid space	1 km (stretched at boundaries)
Vertical grid levels	2, 8, 20, 50, 100, 200, 300, 600, 1000, 2000, 3000, 4000, 6000, 9000
Initial stratification	0.2°K km^{-1}

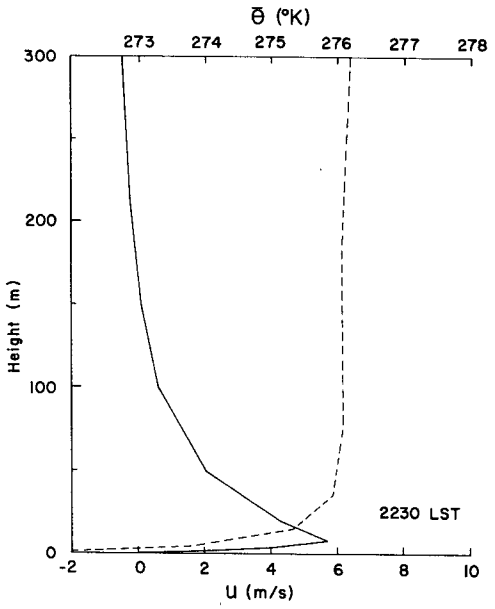

FIG. 2. Downslope component (solid line) and potential temperature (dashed) profiles over the western sidewall of the two-dimensional valley at 2230 LST.

The symbols F_q and F_θ represent source/sink terms for θ and q (e.g., radiational flux divergence). "Fil" denotes a horizontal filter in place of horizontal diffusion. This filter suggested by Paul Long (personal communication, 1983) is implicit and given by

$$(1 - \delta)\phi_{i+1}^{\tau+1} + 2(1 + \delta)\phi_i^{\tau+1} + (1 - \delta)\phi_{i-1}^{\tau+1} = \phi_{i+1}^{\tau} + 2\phi_i^{\tau} + \phi_{i-1}^{\tau},$$

where $\phi_i^{\tau+1}$ is the filtered variable at grid point i and ϕ_i^{τ} is the original value. The δ represents a filter coefficient which determines the amount of smoothing to be accomplished and in the present study was set at 0.08. The above system of algebraic equations can be solved easily with a tridiagonal solver. The filter has the advantage of selectively damping unwanted small wavelength features, thereby controlling aliasing. Mahrer and Pielke (1978) provide a response function and effective filtering as a function of δ and wavelength. As an example the 0.08 value used here essentially removes all $2\Delta X$ waves but $4\Delta X$ waves and larger would retain better than 90% of their original amplitude.

For the nocturnal slope and mountain flows considered in this investigation a rigid top ($s = \bar{s}$) was imposed with fixed boundary conditions at the top. It is felt that this simple boundary condition with the top model level near the stratosphere is adequate for simulating shallow nocturnal drainage flows. Model tests in two-dimensions using both a fixed top and floating material surface at a height of 9 km produced virtually identical slope flow solutions.

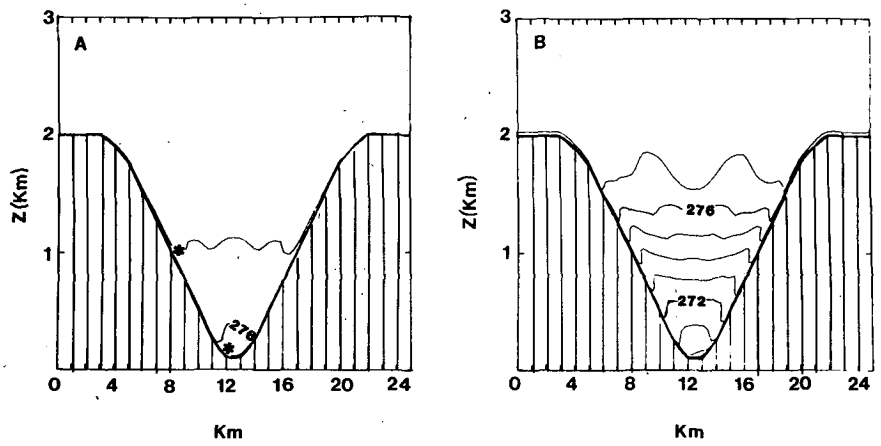

FIG. 3. Contours of potential temperature in the two-dimensional valley. (a) Contours for 2030 LST, (b) Contours for 0230 LST. Contour interval is 1 K. Asterisk gives location for profiles and time series in Figs. 2 and 5.

b. Numerical aspects

Aside from the use of the terrain-following coordinate which allows inclusion of topography in a general manner, several numerical techniques worth noting are utilized in the model. Perhaps the most important is a quasi-Lagrangian spline technique for numerical evaluation of the nonlinear advection terms. This technique, described by Mahrer and Pielke (1978), is highly accurate and reduces substantially the numerical damping associated with some numerical schemes and retains a highly accurate representation of phase speed. A second important technique is the use of an implicit numerical scheme (Paegle *et al.*, 1976) for evaluation of the vertical diffusion terms. This scheme is thought to be especially important for the use of local exchange coefficients described later.

A surface energy budget employing multiple soil layers (Mahrer and Pielke, 1977) is used to force the model. Surface turbulent fluxes are parameterized using the similarity formulas of Businger (1973).

c. Lateral boundary conditions

Specification of proper boundary conditions is always difficult in limited scale modeling. First is the problem of spurious accelerations across the model domain due to erroneous differential specification of boundary values (Anthes and Warner, 1978.) The second, which has received more attention, is wave reflection from the boundaries resulting in amplification and destruction of wave forms. Because of the low initial wind values which will be imposed in studying the valley flow problem and the fact that the thermally induced circulations will gradually spin up, the initial impulsive imbalance and resulting amplitude of the mass adjusting gravity waves and inertial oscillations should be relatively small. (Small in comparison to the size of initial imbalances expected in high speed forced flows over terrain.)

In the present investigation, zero gradient boundary conditions were utilized at all lateral boundaries. The model grid lattice was stretched near the boundary to remove the boundary as far as possible from the region of interest. In addition a buffer zone near the boundaries of at least eight grid points of zero gradient topography was incorporated. Two-dimensional tests indicated interior solutions were not affected substantially by further expansion of the model domain.

These simple boundary conditions cannot, of course, adequately handle pronounced flow reversal at the boundaries nor completely remove the erro-

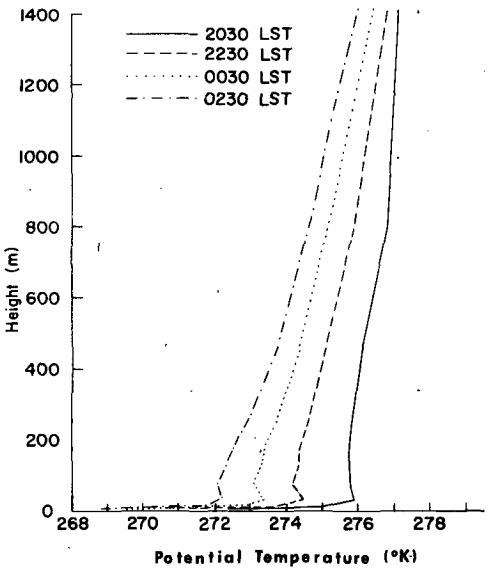

FIG. 4. Profiles of potential temperature over the center of the two-dimensional valley for the indicated times.

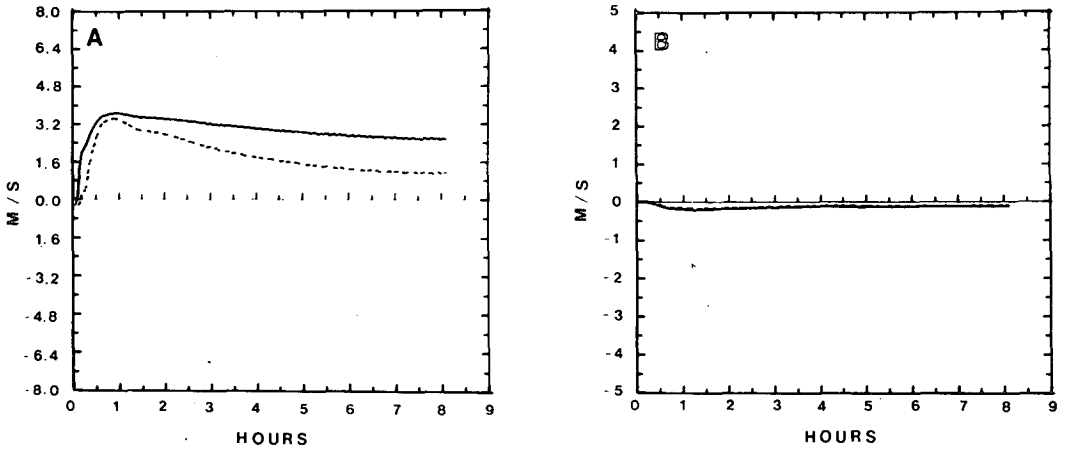

FIG. 5. Time series plot of (a) downslope u-component at two meters (dashed) and 50 meters (solid) above the western sidewall and (b) v-component above the middle of the valley floor. Velocities plotted are three-minute averages.

neous domain accelerations described above. However, it is felt that they are adequate for this first attempt to model idealized valley situations.

d. Boundary layer and radiative formulation

Turbulent exchange processes are critical to the development of nocturnal drainage flows and mountain winds. Not only does turbulent transfer through surface drag and interfacial entrainment govern the speed and depth of the drainage flow; but, the turbulent transport of heat essentially defines the depth and amplitude of the temperature perturbation which directly drives the drainage flow.

While stable boundary layer structure over flat land is complex in its own right, the turbulent structure and behavior is even more complicated in slope drainage flows. For example, in drainage flows, because the accelerations appear at the surface, the turbulent momentum transfer is upward in the shear zone between the slope flow and the ambient flow. This is contrary to the conventional downward transport over a flat stationary boundary. (Nonsteady flows such as inertial oscillations can produce similar transient upward transport of momentum above the nose of a wind maximum.) Also, as will be shown later, downslope and return flows can produce thermal instabilities aloft causing convective instability even though the surface is stable.

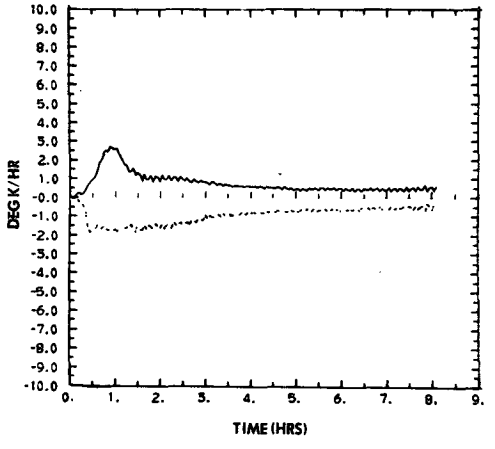

FIG. 6. Time series of local warming (dashed) and advective warming (solid) over the western sidewall. Warming rates are three-minute averages.

Because turbulent mixing properties in drainage flows are not entirely related to surface frictional or stability effects, a turbulent parameterization based upon local conditions (Blackadar, 1979) was chosen for use in the slope and mountain-wind model experiments. Blackadar's formulation makes the turbulent exchange coefficients a function of the departure of the local gradient Richardson number from a critical Richardson number; therefore, shear and stratification influence the magnitude of the exchange coefficient. Thus, the formulation in effect mimics a turbulent energy equation except turbulent transport of turbulent energy is neglected. McNider and Pielke (1981) provide a complete description of the scheme and its numerical application in the present model.

The major advantage to the local formulation over a profile or surface related form is that local changes in thermal stratification through differential thermal advection can be included since the magnitude of the exchange coefficient is dependent upon the local thermal gradient. In the slope flows which follow, differential thermal advection often produces a tendency to cause unstable layers aloft. The local Richardson number scheme, as in the real atmosphere, tends to dissipate these unstable layers through turbulent mixing.

3. Two-dimensional experiments

The valley modeled was purposely accentuated to have a high height-to-width ratio (19 km wide, 2 km deep) with a sidewall slope of 0.25 (14°). Table 1 gives additional details of the model run. Although initial sensitivity studies were carried out using specified constant surface cooling rates, the cases reported here were forced by cooling produced by the surface energy budget. Actual surface cooling rates produced by the budget ranged from approximately 0.5 degrees per hour on the sidewall to 1.5 degrees per hour in the valley center for the first few hours of integration. Later, both sidewall and valley center surface cooling rates approached 0.5 degrees per hour.

a. Sidewall slope flows

The model was started at local sunset (1730) at rest (1 cm s^{-1} imposed velocity) and cooling began immediately. A near-zero synoptic flow was chosen in order to isolate the thermal effects. Also the light wind case is often the most critical to air pollution problems. Shallow drainage flows developed quickly on both valley walls, converging toward the center. A slight return circulation or upslope flow also appeared above the downslope flow. This is shown in Fig. 2 which gives the velocity profile that developed over the center of the western sloping wall along with the temperature profile (see Fig. 3 for the shape of the valley.) As can be seen, the slope flow is strong, but shallow, with the velocity maximum occurring at only 8 meters above the surface. Observations by Defant (reported by Sutton, 1953) over extremely steep terrain showed maximum velocities at approximately 30 meters above the surface. More recent observations (Hosker *et al.*, 1980) taken under the ASCOT program for slopes more nearly similar to those modeled here indicated extremely shallow slope flows with maximum velocities occurring below 3 meters.

b. Valley inversion

As the sidewall slopes cool, the slope flows begin to fill the valley with the cooled air. This is graphically illustrated in Fig. 3 which gives potential temperature contours in the valley. Initially there is only a slight stratification in the valley, while after several hours of slope flow, a deep inversion has formed within the entire valley. The pooling of the cool air is a significant feature in the model solutions, since in Defant's (1951) descriptive model it is the filling of the valley with the cooled air which produces the along-valley axis mountain wind.

The cooling pattern in the valley is quite interesting. As can be seen by the contours in Fig. 3, the cooling

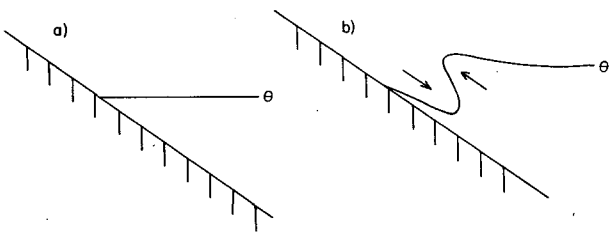

FIG. 7. Schematic of the deformation of the potential temperature field due to downslope and return upslope flow and resulting destabilization. (a) initial profile and (b) after deformation by slope flow.

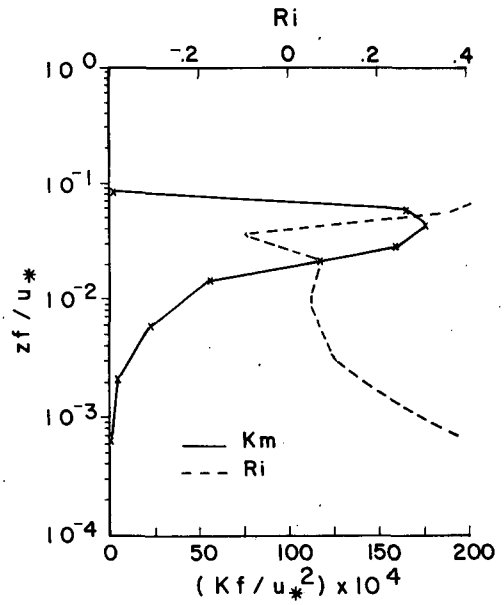

FIG. 8. Turbulent exchange coefficient (solid) over the western valley wall showing pronounced maximum near the top of the slope flow. The dashed line gives the local gradient Richardson number showing the unstable layer aloft created by the deformation illustrated in Fig. 7.

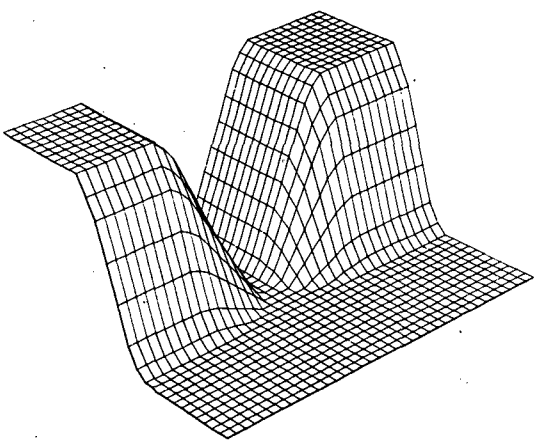

FIG. 9. Three-dimensional perspectives of the topographic configuration used in Case A. Ridge height is 2 km; valley width is 19 km. (Note that the vertical scale is exaggerated.)

occurs at essentially all heights. This is also demonstrated in Fig. 4 which gives temperature profiles over the center of the valley as a function of time. Although this shows that more cooling does occur at the surface, the entire profile within the valley is cooled with time. This cooling pattern is consistent with that observed in deep valleys in the Rockies (Whiteman and McKee, 1977).

Partitioning of the model cooling into radiative, turbulent and advective components shows that the cooling in the valley is almost entirely due to advective processes. The advective cooling is perhaps counter to first intuition in that it is positive vertical motion over the center of the valley rather than downward flow over the valley sidewalls which leads to the cooling in the upper reaches of the valley. As shown by Blackadar (personal communication, 1982) and McNider (1982), sidewall advection in a stably stratified environment can only lead to warming, i.e.,

$$\frac{\partial \theta}{\partial t} = -w \frac{\partial \theta}{\partial z} > 0$$

for flow down the sidewalls. Over the center of the valley convergence and upward vertical motion lead to a divergence in isentropes. Thus the sidewall flows do not provide any additional net cooling in the valley and only through their convergence and increased turbulent mixing redistribute the radiatively cooled air near the bottom of the valley.

c. *Time dependence of the slope flows*

As mentioned, the slope flows developed very quickly in response to the cooling, reaching a maximum velocity over the center of the slope of approximately 6 m s^{-1} after 45 minutes of cooling. Afterwards velocities decreased through the night, finally reaching a near steady state after seven hours. Figure 5 shows a time plot of the slope flows at two meters and 50 meters above the middle of the western slope and the along-valley flow over the center of the valley.

The velocities evidently decrease in part due to the increasing temperature stratification occurring in the valley. This is consistent with analytical solutions (McNider, 1982) in which the downslope velocities were found to be inversely proportional to the strength of the stratifications.

Two factors, both related, also contribute to the decreasing velocity. First, the cooling rate over the slope begins to decrease as a balance develops between local cooling (radiational and turbulent) and advective warming due to the developing stratification. This is illustrated in Fig. 6 which gives the local and advective contributions to the cooling above the slope. (The short-period fluctuations seen in the figure are turbulent bursts due to Richardson number instability discussed in the next section.) Second, the cooling over the center of the valley, due to the pooling of cool air, reduces the horizontal temperature gradient which directly drives the slope flows.

d. *Turbulent structure*

The turbulent exchange processes in the slope flows are directly linked to the developing flow field and are much more complicated than the boundary layer processes occurring over flat land. The first reason for this complexity is that cooling is greatest near the surface so that the slope flow accelerations are strongest there. Thus a region of negative wind speed shear occurs above the surface causing turbulent momentum transfer to be upward rather than downward in the upper part of the slope flows. This is contrary to steady flat terrain boundary layer structure. Second, the modeled slope flows perturb the potential tem-

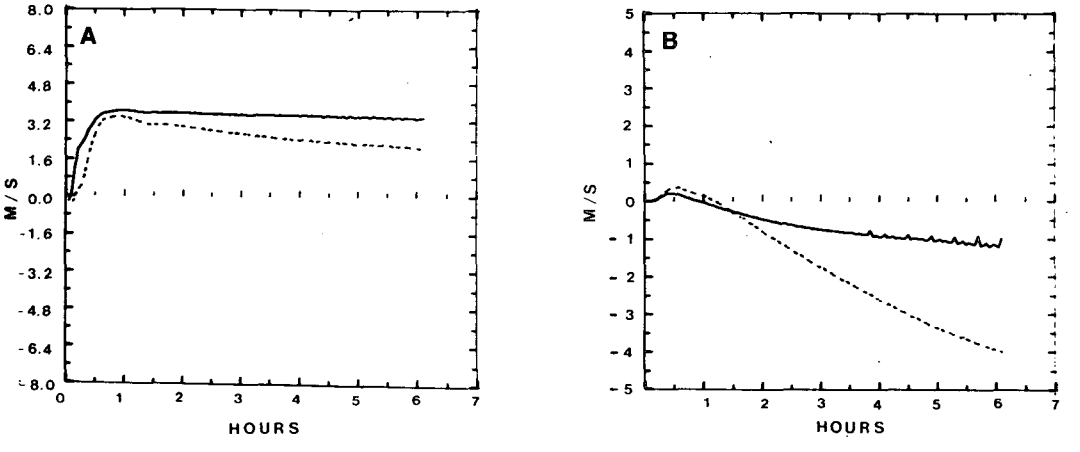

FIG. 10. (a) Times series of u-component at 2 meters (solid) and 50 meters (dashed) over the middle of the western sidewall ($x = 15$, $y = 23$). (b) Times series of v-component at 2 meters (solid) and 50 meters (dashed) at the center of the valley ($x = 18$, $y = 23$).

perature structure, thus destabilizing the boundary layer creating high turbulent levels aloft.

This second factor is a fundamental difference in the way boundary layers behave in inhomogeneous settings where differential advection takes place. This appears to have been neglected in other slope flow investigations, since a two-dimensional dynamic model with turbulent exchange processes dependent on local conditions is needed to exhibit this characteristic. Physically the downslope flows, through advection processes, deform the potential temperature field creating a less stable profile. The upslope flow further deforms the field actually producing an unstable profile. This deformation is shown schematically in Fig. 7 and is also visible in the contours of potential temperature in Fig. 3.

Because turbulent exchange in the model is dependent upon the local Richardson number, the destabilized temperature profile in conjunction with wind shear between the downslope and upslope flows produces a highly turbulent region aloft. Figure 8 gives the turbulent exchange coefficient over the slope along with the local gradient Richardson number. In the face of the flow field continually destabilizing the temperature profile, the high level of turbulence tries to create a near-adiabatic profile removing the instability. This is seen in the temperature profile in Fig. 2. Despite the high level of mixing the unstable layer is persistent even in hour-averaged profiles, as can be seen in Fig. 4. This illustrates that the differential advection is occurring at a faster rate then the Richardson number dependent exchange coefficient can remove the instability. The profile of exchange coefficients in Fig. 8 has a larger amplitude and different slope than over a flat boundary.

The complex thermodynamic and shear structure in the slope flows emphasizes the importance of using turbulent parameterization dependent upon local conditions. Although this discussion has centered upon the role of the slope flows in producing the turbulent structure, it must be remembered that it is also the turbulent exchange processes which determine the depth and strength of the slope flows. Because of the complexity of the system, it is likely that even more sophisticated or higher-order turbulence models may be needed to properly describe the subtleties of the problem.

4. Idealized three-dimensional slope and mountain flows

While the previous section provided a description of the characteristics of the two-dimensional slope flows, the mountain wind or the along-valley axis component is a three-dimensional feature, directly coupled to the sidewall slope flows. The following case study is designed to investigate the pooling of the cooled air in a three-dimensional valley and development of the mountain wind (in the along-valley axis wind) in response to the pooled air.

The case study utilizes a three-dimensional counterpart to the two-dimensional valley described earlier. Figure 9 gives a three-dimensional perspective of the topography which is essentially the classic valley–plain configuration considered in the descriptive model of Defant (1951). The north end cross-section corresponds to the two-dimensional cross-section utilized in the previous section. Grid spacing is 1 km in east–west direction and 2 km in the north–south direction except at the boundaries where the grid is

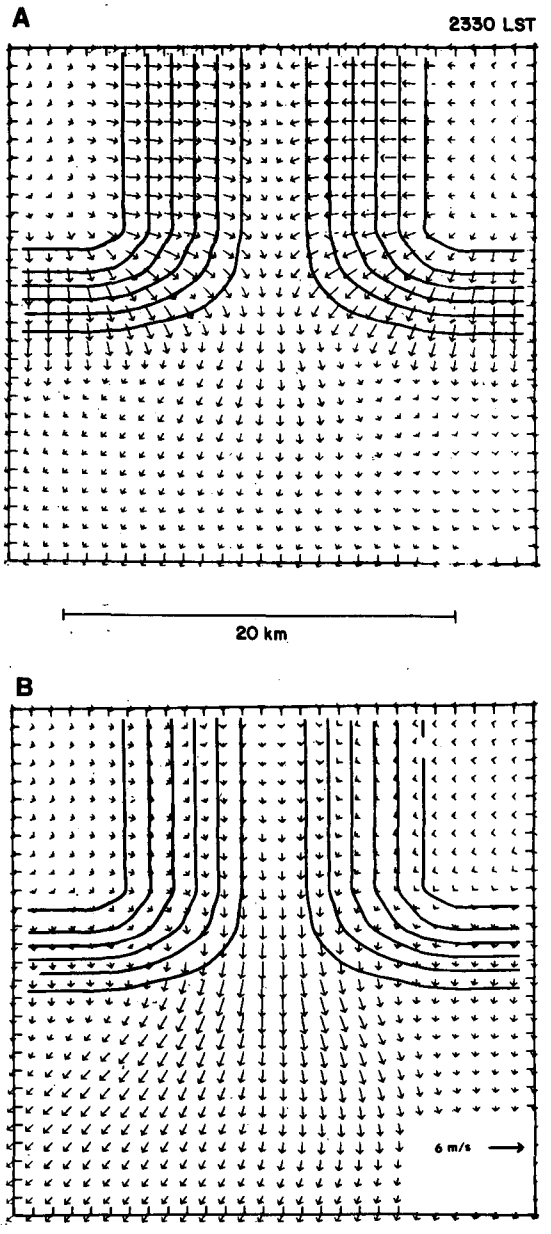

FIG. 11. Plan view of velocity field for Case A at 2330 LST, (a) at z^* level of 8 meters and (b) at z^* level of 100 meters.

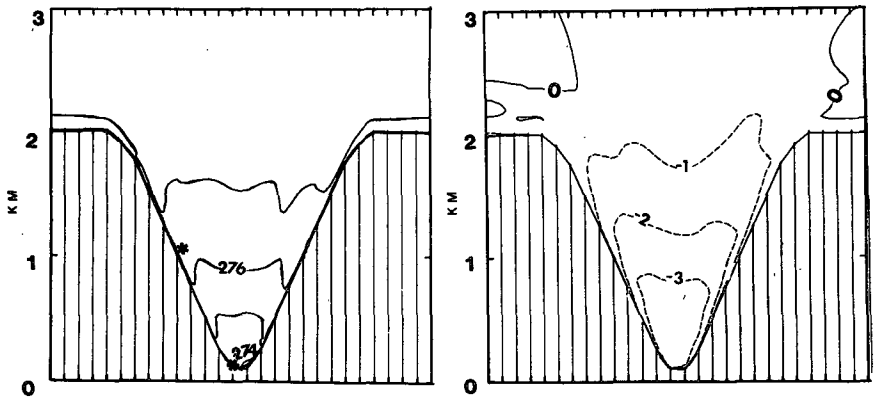

FIG. 12. (a) Contours of potential temperature at 2330 LST (y = 23). Contour interval is 1 K. (b) Contours of the mountain wind (v-component) for the same time and location. Contour interval is 1 m s^{-1}.

stretched by 1 km per grid for 5 grids. Because zero gradient boundary conditions are utilized at the lateral boundaries, the topography corresponds to an infinite valley extending to the north and a flat plain extending infinitely toward the south. Note that the valley floor does not slope toward the plain. The model parameters are the same as those given in Table 1 in the previous section.

The model was started at sunset with a near adiabatic initial state and was run for seven hours. (For the idealized 3-D simulations, approximately five minutes of CRAY-1 time was required per hour of simulation.) As in the two-dimensional cases, the slope flows start almost immediately and begin to converge at the valley center. Slope flows also develop over the slopes leading onto the plain. The profiles of the downslope component were virtually identical to those given in the two-dimensional case. Cool air began to pool in the center of the valley as in the two-dimensional runs; however, in the three-dimensional case a true mountain wind from the valley to the plain began to develop. Figure 10 shows the time-dependent development of both the slope flow (u-component) and mountain wind (v-component) and can be compared to the two-dimensional run (Fig. 5) in which no significant v-component developed. As can be seen in the figure, the mountain wind does not begin immediately and lags the development of the slope flows by approximately one hour. Also the flow toward the plain is entirely due to the pooling of the cold air, since no slope exists in the valley floor.

Figure 11 shows a vector plot of the model flow field at two selected levels. As can be seen, the flow near the surface moves down the valley sidewalls, converges in the center and flows out the valley. At the higher level within the valley the flow is almost totally in the along-valley direction moving out over the plain. The slight asymmetry is due to Coriolis turning.

Figure 12 gives contours of the mountain wind (v-component) at a cross-section of the valley after six hours. The mountain wind is pervasive and fills almost the entire valley. The development of the deep mountain flow in the third dimension is consistent with the observations of Davidson and Rao (1963) and the descriptive ideas of Defant (1951). For comparison with the model, Fig. 13 gives the wind observed by Buettner and Thyer (1966) in the Carbon River Valley near Mt. Ranier in Washington.

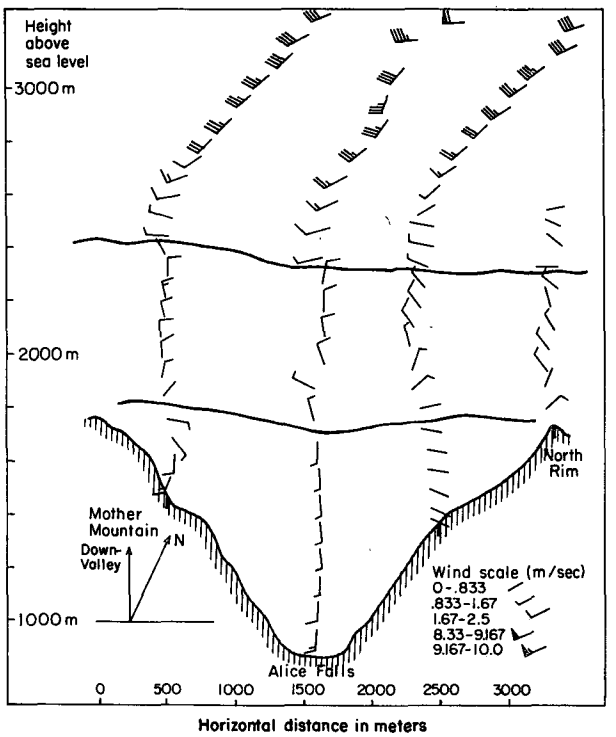

FIG. 13. Observations of a mountain wind reported by Buettner and Thyer (1966) in the Carbon River Valley at 0500 LST 9 July 1959.

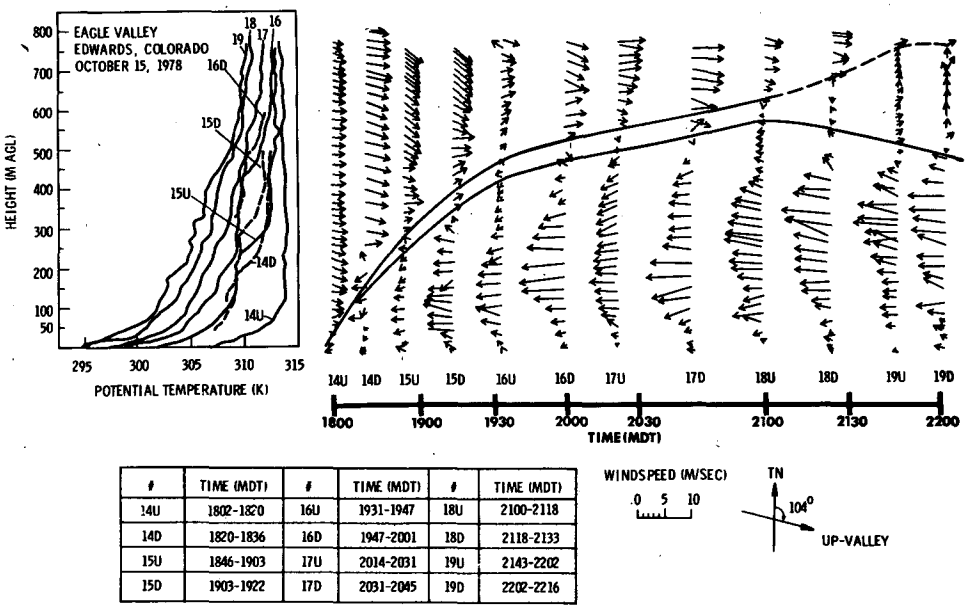

#	TIME (MDT)	#	TIME (MDT)	#	TIME (MDT)
14U	1802-1820	16U	1931-1947	18U	2100-2118
14D	1820-1836	16D	1947-2001	18D	2118-2133
15U	1846-1903	17U	2014-2031	19U	2143-2202
15D	1903-1922	17D	2031-2045	19D	2202-2216

FIG. 14. Observations of valley inversion and mountain flow development in the Gore–Eagle Valley System by Whiteman (1981). Wind vectors give time series of horizontal wind over the center of the valley. U and D indicate up and down tethersonde ascents. Note the deep down-valley flow oriented almost directly along the valley axis. Model results for comparison are given in Fig. 13.

As can be seen the down valley flow completely fills the valley in agreement with Defant's ideas and the model. The observations show the maximum down-valley flow occurs near the surface, whereas the model shows the maximum velocity near or to mid-depth. This is apparently due to the slope in the valley floor in the observation which is not included in the idealized topography used in the model.

As can be seen in Fig. 12 a significant upvalley or anti-wind, as described by Thyer (1966), is not present above the mountain wind. This is because of the two-dimensional characteristics of the topography in that there is no valley head. Also, the plateau configuration above the valley sides can provide the mass feeding the slope flows. A slight up-valley return circulation is noted above the sidewall plateau by the existence of the zero contour line. Thus, for this topography the anti-wind required by mass continuity does not occur over the mountain wind, but, to the sides over the plateau supporting the mass required by slope flow.

5. Model application to actual topography and comparison with observations

High quality representative observational data in complex terrain available for testing the model prediction of slope and mountain flows are scarce, thus model evaluation in the previous two sections was limited to comparison with descriptive models (e.g., Defant, 1951). It should be remembered, however, that these descriptive models are, in fact, a synthesis

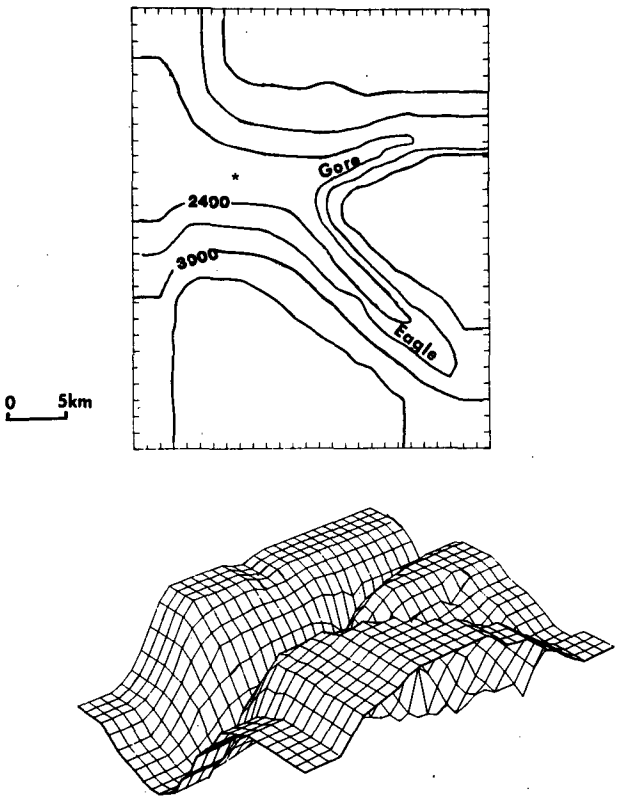

FIG. 15. Contour map and three-dimensional perspective of the topography utilized in the simulation of the Gore–Eagle Valley System. The asterisk shows the approximate point of observations by Whiteman given in Fig. 14 and model results given in Fig. 17. Contour interval is 200 meters.

or composite of many observations so that they are perhaps more representative of average valley meteorology than isolated observational data which can be unduly influenced or contaminated by local small-scale topography or other larger-scale phenomenon (e.g., sea breezes, large-scale topographic flows). A major use, however, of a numerical model (besides its use in understanding phenomena) is simulation of discrete events which requires evaluation of model skill in reproducing single sets of observations. Although recent extensive field programs by the Department of Energy (ASCOT) and the Environmental Protection Agency have taken place in complex terrain, their data to date have addressed fundamentally different phenomenon (e.g., slope flows, flow over obstacles, etc.) than the three-dimensional deep mountain flows addressed here. The data sets most applicable to deep mountain flows are those taken by McKee, Whiteman and associates at Colorado State University in deep, well-defined Colorado valleys (e.g., Whiteman and McKee, 1977).

In order to evaluate the models in this mode, the numerical model was applied to simulate a set of observations reported by Whiteman (1981) for the Gore–Eagle Valley System in Colorado. The observations by Whiteman for 15 October 1978 illustrate an apparent classical case of the development of a valley inversion and subsequent deep mountain wind. Figure 14 from Whiteman (1981) shows the development of the thermal structure and flow regime in the valley. The figure shows a time series of horizontal wind vectors at a point in the center of the valley. Figure 15 shows both a contour map and three-dimensional perspective of the topography utilized in the simulation. The approximate observation point for Fig. 14 is indicated on the contour map. The topography, as shown, was smoothed and adjusted to zero gradient at the boundaries in conformity with the lateral boundary conditions in the model. The smoothed topography maintains the basic height-to-width ratio of the actual valleys, sidewall slopes and valley floor slopes.

The model was run beginning at sunset (1737 MDT) and initialized at the lower levels (below 1 km) with a near-adiabatic thermal structure consistent with the potential temperature profile reported by Whiteman from tethersonde data. Upper level thermal and moisture data were taken from the Grand Junction, Colorado, National Weather Service upper air soundings located 180 km west-southwest of the valley site.

A high pressure area was centered over the area and upper-level winds were weak. Model winds were initialized using the lower-level winds reported from the tethersonde data at (1802–1820 MDT) which showed a light (2.5 m s^{-1}) wind from the west. As in the previous cases, sidewall slopes began to cool producing slope flow converging in the center of the valley. This is illustrated in Fig. 16 which shows low-level flows essentially following the topographic fall vector. Gradually, due to the valley cooling processes cited in Section 2b, a deep inversion develops in the valley, as can be seen in Fig. 17. Comparison of the developing temperature structure in the model to the observations indicates that while some advective cooling occurs aloft, the model inversion is both weaker and shallower than observations. Possible reasons for the lack of elevated cooling will be discussed later.

Figure 17 shows the development of the flow structure over the center of the valley which can be compared to Fig. 14. The model produces the observed development of the deep along-valley axis down-

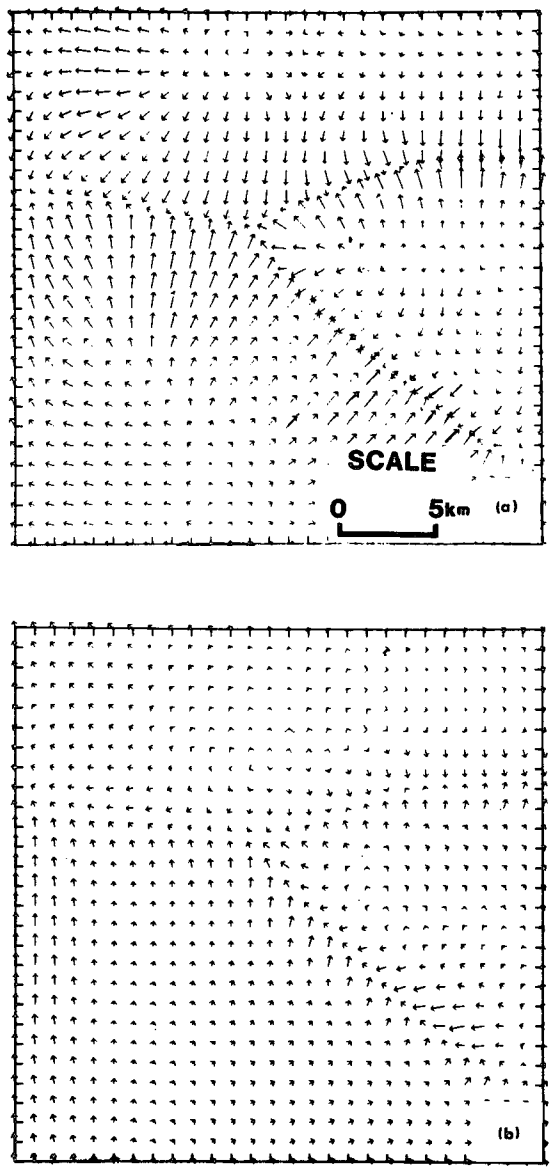

FIG. 16. Vector depiction of model flow field at 2330 LST (a) at a height of 5 meters and (b) at a height of 50 meters.

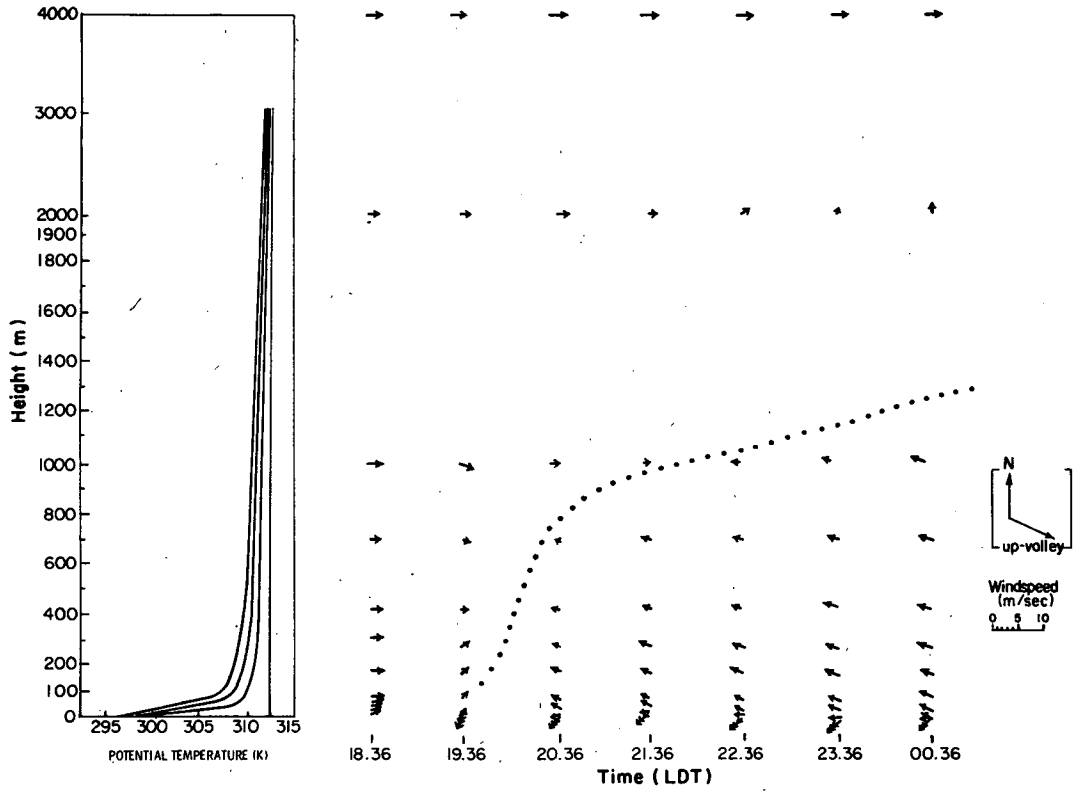

FIG. 17. Model predicted development of temperature structure over the center of the valley at 2-hour intervals beginning at 1837 LDT (local daylight time) and the horizontal wind over the center of the valley. For comparison with observations, see Fig. 14.

valley flow in opposition to the imposed synoptic wind. While the model results show good qualitative agreement with the observations in terms of the along-valley axis flow and the growth of this flow, the strength of the down-valley flow is underestimated ($\approx$3 m s^{-1} versus $\approx$7 m s^{-1}) and the model flow is much deeper. The shallow slope flows apparent near the surface along the valley floor in the model are, in part, due to discretization of the topography, i.e., with a coarse grid (1 km) sidewall slope exists in the model which is absent in the actual flat bottom of the valley.

Although the model results are encouraging, some significant differences do exist between the model and observations. The basic problem appears to be specification of lateral boundary conditions. Implicit in setting boundaries is the assumption that topographic features outside of the model domain do not influence the interior solution. In the present study case this may not be valid in that the zero-gradient boundary conditions used in the model imply that the Gore Valley extends infinitely to east. Thus, the imposed westerly synoptic wind can sweep through this valley, carrying any accumulated cold air to the east with no blocking effect. In actuality, a definite valley head exists in the Gore Valley, similar to the valley head incorporated in the Eagle Valley. Thus, eventually a back pressure would develop and the cold air accumulation would remain in the valley. This could greatly accentuate the pressure head between the interior of the valley and the opening to the west, thus increasing the strength of the inversion and of the valley flows over that which was modeled.

6. Summary and conclusions

The major features of the classic mountain–plain circulation, including the deep mountain flow out of the valley are simulated using a numerical three-dimensional model. The mountain flow unlike direct sea breeze circulations or slope flows is a secondary circulation and is dependent upon the slope flows and three-dimensional geometry of the valley. While the numerical model appeared to reproduce qualitatively the structure of the descriptive model of Defant (1951), application to a specific data set for the Gore–Eagle Valley in Colorado indicated that the model underestimated the strength of the mountain flow and overestimated the depth of the flow.

The two-dimensional cross-valley circulations simulated in the present study point out differential advection as a mechanism for maintaining high tur-

bulent levels aloft in slope flows in spite of strongly stratified conditions at the surface. This mechanism also underlines the importance of including local dependence in turbulence in models as opposed to profile formulations based on surface characteristics. The model studies further show that cooling of the valley atmosphere occurs due to upward vertical motion over the center of the valley, not due to direct downslope flow from the slopes.

Acknowledgments. This research was supported by the U.S. Environmental Protection Agency, the National Park Service and National Science Foundation Grant ATM8304042. This work does not necessarily reflect U.S. EPA policy. Computer support by the National Center for Atmospheric Research was funded by the National Science Foundation. The authors appreciate the helpful advice of their colleagues Bob Kessler, Mike McCumber and Moti Segal. The authors wish to thank Doshia Mitchell and Valerie Seaquist for their help in manuscript preparation.

APPENDIX

List of Symbols

c_p	specific heat at constant pressure
f	Coriolis parameter
g	acceleration of gravity
h	height of surface layer
k_0	von Karman's constant
K_s	soil heat diffusivity
K_m, K_h	vertical exchange coefficient of momentum and heat
p	pressure
p_{00}	reference pressure
q	specific humidity
R	gas constant for dry air
$\bar{s}$	initial height of the material surface
s	material surface top of the model
T	temperature
u, v, w	east–west, north–south initial wind component of velocity
U_g, V_g	east–west and north–south geostrophic wind
u_*	surface friction velocity
w^*	vertical (z^*) component of velocity
x, y, z	Cartesian coordinates
z^*	vertical, terrain-following coordinate
z_G	ground elevation
z_0	roughness parameter
z_i	depth of planetary boundary layer
$\tilde{\pi}$	Exner's function = $c_p(P/P_{00})^{R/c_p}$
θ	potential temperature
θ_*	surface friction temperature

Subscripts G and s denote ground and soil values respectively.

REFERENCES

Anthes, R. A., and T. Warner, 1978: Development of hydrodynamic models for air pollution and other mesometeorological studies. *Mon. Wea. Rev.*, **105**, 1045–1078.

Blackadar, A. K., 1979: High resolution models of the planetary boundary layer. *Advances in Environmental and Scientific Engineering*, Vol. 1, Gordan and Breach, 50–81.

Brost, R. A., and J. C. Wyngaard, 1978: A model study of the stably stratified planetary boundary layer. *J. Atmos. Sci.*, **35**, 1427–1440.

Buettner, K. J. K., and N. Thyer, 1966: Valley winds in the Mount Ranier area. *Arch. Meteor. Geophys. Bioklim.*, **B14**, 125–147.

Businger, J. A., 1973: Turbulent transfer in the atmospheric surface layer. *Workshop on Micrometeorology*, Boston, Amer. Meteor. Soc., 392 pp.

Davidson, B., and P. K. Rao, 1963: Experimental studies of the valley-plain wind. *Int. J. Air Wat. Pollut.*, **7**, 907–923.

Defant, F., 1951: Local winds. *Compendium of Meteorology*, T. J. Malone, Ed., Amer. Meteor. Soc., 655–675.

Delage, Y., 1974: A numerical study of the nocturnal atmospheric boundary layer. *Quart. J. Roy. Meteor. Soc.*, **100**, 351–364.

Egger, J., 1981: Thermally forced circulations in a valley. *Geophys. Astrophys. Dyn.*, **17**, 255–279.

Hosker, R. P., K. S. Rao and G. A. Briggs, 1980: Experimental methods and preliminary analyses of drainage flow observations during the first ASCOT field study. *Second Joint Conf. on Applications of Air Pollution Meteorology, New Orleans, Amer. Meteor. Soc.*, 870 pp.

Mahrer, Y., and R. A. Pielke, 1977: The effects of topography on land and sea breezes in a two-dimensional mesoscale model. *Mon. Wea. Rev.*, **105**, 1152–1162.

——, and ——, 1978: Test of an upstream spline interpolation technique for the avective terms in a numerical mesoscale model. *Mon. Wea. Rev.*, **106**, 818–830.

McCumber, M. C., and R. A. Pielke, 1981: Simulation of the effects of surface fluxes of heat and moisture in a mesoscale numerical model. *J. Geophys. Res.*, **86**, 9929–9938.

McNider, R. T., 1982: A note on velocity fluctuations in drainage flows. *J. Atmos. Sci.*, **39**, 1658–1660.

——, and R. A. Pielke, 1981: Diurnal boundary layer development over sloping terrain. *J. Atmos. Sci.*, **38**, 2198–2212.

Paegle, J., W. G. Zdunkowski and R. M. Welch, 1976: Implicit differencing of predictive equations for the boundary layer. *Mon. Wea. Rev.*, **104**, 1321–1324.

Pielke, R. A., 1974: A three-dimensional numerical model of the sea breezes over south Florida. *Mon. Wea. Rev.*, **102**, 115–139.

——, and C. L. Martin, 1981: Consistent derivation of a terrain-following coordinate system for use in a hydrostatic model. *J. Atmos. Sci.*, **38**, 1707–1713.

Sutton, O. G., 1953: *Micrometeorology*, McGraw-Hill, 333 pp.

Thyer, N. H., 1966: A theoretical explanation of mountain and valley winds by a numerical method. *Arch. Meteor. Geophys. Bioklim.*, **15**, 318–348.

Whiteman, C. D., 1981: Temperature inversion buildup in valleys of the Rocky Mountains. *Second Conf. on Mountain Meteorology*, Steamboat Springs, Amer. Meteor. Soc., 408 pp.

——, and T. B. McKee, 1977: Observations of vertical atmospheric structure in a deep mountain valley. *Arch. Meteor. Geophys. Bioklim.*, **26**, 39–50.

Yamada, T., 1981: A numerical simulation of nocturnal drainage flows. *J. Meteor. Soc. Japan*, **59**, 108–122.